

pubs.acs.org/IECR Article

# Characterizing Polyvinyl Chloride Interactions with Additives in Traditional and Bioderived Solvents

Feranmi V. Olowookere, Gabriel D. Barbosa, and C. Heath Turner\*



Cite This: Ind. Eng. Chem. Res. 2024, 63, 1109–1121



**Read Online** 

**ACCESS** 

III Metrics & More

Article Recommendations

sı Supporting Information

ABSTRACT: We conduct a comprehensive investigation into the interactions between polyvinyl chloride (PVC) and its additives, with a focus on exploring alternative, bioderived solvents for processing PVC waste. Using molecular simulations, we evaluate the performance of five bioderived solvents and compare them against other traditional solvents, such as tetrahydrofuran (THF) and ethyl acetate (ETA). We examine the impact of the different solvents on the physical and mechanical properties of PVC, as well as their propensity to solvate PVC and its additives. Our findings suggest that bioderived solvents may provide comparable, if not superior, PVC solvation performance relative to traditional solvent formulations, highlighting these compounds as potential eco-friendly alternatives. Future experimental studies are planned to validate these findings and assess the practicality of these bioderived solvents, considering factors such as cost, synthesis feasibility, and toxicity.



# 1. INTRODUCTION

Polyvinyl chloride (PVC) is one of the most versatile and widely used polymers in the modern world due to its tunable properties, affordable manufacturing processes, and resistance to degradation.<sup>1,2</sup> The robust performance of PVC-based materials is partially attributed to the incorporation of various additives,<sup>3</sup> including roughly 500 varieties of plasticizers,<sup>4</sup> as well as heat stabilizers and flame retardants, making up 30% and 12% of the PVC additive demand, respectively.5 The urgent need to recycle and/or upcycle PVC materials is complicated by the environmental implications of the aforementioned additives, which harm marine life by disrupting the metabolism of different organisms<sup>7-9</sup> and strongly attracting heavy metals such as copper and zinc. 10 As sustainable end-of-life disposal, reuse, and upcycling of PVC intensifies, 11 it is imperative to quantify PVC-additive interactions and develop a better molecular-level understanding of alternative solvent formulations for processing end-of-life PVC materials.

Experimental studies of PVC additives help elucidate their behavior and broad influence on PVC properties,  $^{5,12-16}$  with certain fillers (e.g., SiC and  $Al_2O_3$ ) enhancing wear resistance and others (e.g.,  $CaCO_3$ ) impeding it.  $^{14}$  Interestingly, PVC foams, when modified with  $CaCO_3$ , can be ideal for specific applications like plant watering or home construction.  $^{15}$  Yet, caution is warranted as certain additives (e.g., diarylide yellow) can produce toxic byproducts at high temperatures.  $^{16}$ 

Molecular dynamics (MD) simulations can be used to complement the experimental investigations <sup>13,17</sup> by revealing characteristics emerging from the molecular-level interactions and features within polymer systems, such as the fractional free

volume, relaxation phenomena, glass transition temperature  $(T_{\rm g})$ , and heat of mixing—details often challenging or time consuming to obtain from experiments. However, simulations of polymer—additive—solvent mixtures are relatively rare, with limited studies focusing on the characterization of plasticizers and their influence on the mechanical performance of PVC.  $^{13,17-19}$ 

The shift toward increased sustainability has highlighted the need for improved bioderived solvents for polymer processing. 11,20-22 Recently, Soyemi and Szilvási 23 computationally screened a large library of 9587 different glycerol-based molecules as potential bioderived solvents for plastic waste upcycling (some of which have been experimentally synthesized<sup>24</sup>). Biomass-derived glycerol is produced in large volumes as a side product of biodiesel production, and it is often treated as a waste, so there is a strong need to retain this carbon resource. To initially screen the glycerol-based solvent performance, the previous study employed quantum mechanical calculations and machine learning to determine the relative energy difference (RED) values for each candidate molecule, using the Hansen solubility parameters (HSP).<sup>25</sup> For any two molecules (e.g., PVC and a solvent), their HSP-based similarity Ra, is given by

Received: October 29, 2023 Revised: December 7, 2023 Accepted: December 11, 2023 Published: January 2, 2024





$$Ra^{2} = 4(\delta_{D1} - \delta_{D2})^{2} + (\delta_{P1} - \delta_{P2})^{2} + (\delta_{H1} - \delta_{H2})^{2}$$
(1)

where  $\delta_{Di}$ ,  $\delta_{Pi}$ , and  $\delta_{Hi}$  represent the dispersion, polar, and hydrogen bonding solubility components of each compound, respectively. From this, RED is defined as Ra/R0, where R0 signifies the encompassing radius in the HSP space, experimentally determined based on the "good solvents" for PVC. Therefore, lower RED values could suggest higher compatibility between PVC and a solvent.<sup>26</sup>

In this work, bioderived solvents having a wide range of RED values are investigated (to broadly sample the range of chemical structures studied in literature<sup>23,24</sup>). Through detailed MD simulations, we predict the influence of these solvents on the structural and thermomechanical stability of PVC, comparing their effectiveness to traditional PVC solvents such as tetrahydrofuran (THF), which serve as performance benchmarks. These simulations guide our analyses, offering important guidance for the further design of superior bioderived PVC solvents.

#### 2. SIMULATION DETAILS

2.1. Methods and Models. In our MD simulations, the bonded and nonbonded interaction parameters for PVC, additives, and solvents were represented by the OPLS-AA force field.<sup>27</sup> The atomic charges for PVC were derived using the ab initio Hartree-Fock method using the STO-3G basis set<sup>28</sup> in PolyParGen,<sup>29</sup> while the atomic charges for the solvent and additive molecules were acquired using the 1.2\*CM5 charge method, 30 based on the optimized molecular structures obtained using density functional theory (DFT) calculations at the B3LYP/6-31++(d,p) level of theory. <sup>31</sup> As explicitly shown by Dodda et al., 30 the combination of the 1.2\*CM5 charge method and OPLS-AA force field closely matches experimental results in pure liquid simulations. Furthermore, the choice of these charge methods and basis sets in this study was informed by the need to provide a good balance between accuracy and computational efficiency for the respective molecules.<sup>32–34</sup> Gaussian09<sup>35</sup> was used to perform all of the quantum chemical calculations.

In the MD simulations, a PVC<sub>120</sub> model (i.e., 120 repeat units) was used, since our previous study<sup>36</sup> indicated this to be a reliable atomistic chain length, capable of adequately capturing the general behavior and physics of longer PVC chains. The initial configurations for the MD simulations, shown in Figure 1, were built using the PACKMOL package.<sup>37</sup> We selected specific additives based on their prevalence in commercial PVC applications, <sup>13,38</sup> and they are classified as either plasticizers, flame retardants, pigments, or stabilizers. A comprehensive list of different simulation compositions and labels for the additives and solvents can be found in Table 1, and the molecules are illustrated in Figure 2. These system concentrations were used in order to obtain the same approximate box volumes in the simulations.

All MD simulations were executed using the Gromacs 2021.1 package, <sup>39</sup> and the Visual Molecular Dynamics (VMD) software package <sup>40</sup> was employed for visualization. After building the initial configurations, we optimized the systems using the steepest descent minimization technique to eliminate the potential instabilities. The systems were subjected to an equilibration phase in the isothermal—isobaric (NPT) ensemble at 1 bar and 300 K for 50 ns. To maintain the temperature and pressure, we applied the velocity-rescaling

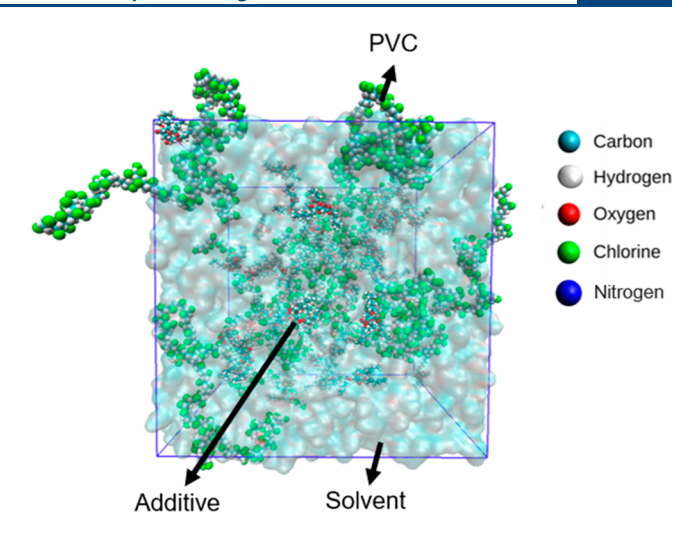


Figure 1. Snapshot of the PVC-additive (CITRA)-solvent (S10) system.

thermostat<sup>41</sup> and the Parrinello-Rahman barostat.<sup>42</sup> An annealing procedure was then applied to each system at a high temperature (600 K) in the NPT ensemble. It was then cooled to 300 K across seven cycles of 60 ns and subsequently equilibrated for an additional 20 ns at 300 K before the production phase was run for 30 ns. Throughout the production run, properties such as RDFs were evaluated with data points gathered at 30 ps intervals. We employed a blockaveraging method with 5 ns sub-blocks to determine statistical uncertainties. The force field involved a Lennard-Jones potential for van der Waals interactions, a 1.0 nm cutoff radius, and geometric combination rules for unlike pair interactions. Long-range electrostatic interactions were computed using the particle mesh Ewald (PME) method<sup>43</sup> beyond a cutoff radius of 1.0 nm. The LINCS algorithm<sup>44</sup> constrained hydrogen bond lengths. The leapfrog algorithm integrated the equations of motion with a 2 fs time step, and periodic boundary conditions were applied in all dimensions.

We further examined the mixing thermodynamics and stress—strain profiles of PVC in both traditional and bioderived solvents (S10, S11, S12, S13 and S14) taken from studies by Soyemi et al.<sup>23</sup> and Chatterjee et al.<sup>24</sup> The system compositions at solvent mass concentrations of 10%, 50%, and 80% are detailed in Table 2.

**2.2. Simulation Analyses.** A viable bioderived solvent should impart a high PVC surface area, indicating good chain disentanglement, as well as a diminished Young's modulus, implying mechanical disruption. Also, the solvent should reduce the interactions between PVC and its additives, which can be quantified by a decrease in the g(r) values of the RDF between specific sites. We first quantify the interaction of typical additives with PVC, followed by an analysis of the solvation of PVC and its additives within five bioderived solvents versus THF (our primary benchmark).

The RDFs and surface area (SA) values were obtained using the Gromacs package tools  $gmx\ rdf$  and  $gmx\ sasa$ , while the  $R_g$  values were obtained using the Plumed package. The stressstrain profiles were obtained using nonequilibrium molecular dynamics (NEMD) simulations in Gromacs, where the system was deformed in the x-direction at a rate of  $10^{-4}$  nm/ps using an anisotropic coupling method. The pressure was kept constant in the orthogonal dimensions (y and z) at a value of 1 bar using a compressibility of  $4.5 \times 10^{-7}$  bar<sup>-1</sup>. In order to

Table 1. Summary of Simulated System Compositions<sup>a</sup>

		PVC	Additive	Solver
PVC-additive	PVC-CITRA	20	90	_
	PVC-DEHA	20	100	_
	PVC-DIOP	20	96	_
	PVC-BRO	20	52	_
	PVC-PHO	20	102	_
	PVC-PIG	20	56	_
	PVC-EPOXY	20	92	_
	PVC-DIST	20	52	_
PVC-solvent	PVC-THF	10	_	700
	PVC-S10	10	_	400
	PVC-S11	10	_	400
	PVC-S12	10	_	400
	PVC-S13	10	_	400
	PVC-S14	10	_	400
PVC-additive-solvent (THF)	PVC-CITRA	10	45	700
	PVC-DEHA	10	50	700
	PVC-DIOP	10	48	700
	PVC-BRO	10	26	700
	PVC-PHO	10	51	700
	PVC-PIG	10	28	700
	PVC-EPOXY	10	46	700
	PVC-DIST	10	26	700
PVC-additive-solvent (S10, S11, S12, S13, and S14)	PVC-CITRA-(S10/S11/S12/S13/S14)	10	45	400
	PVC-DEHA-(S10/S11/S12/S13/S14)	10	50	400
	PVC-DIOP-(S10/S11/S12/S13/S14)	10	48	400
	PVC-BRO-(S10/S11/S12/S13/S14)	10	26	400
	PVC-PHO-(S10/S11/S12/S13/S14)	10	51	400
	PVC-PIG-(S10/S11/S12/S13/S14)	10	28	400
	PVC-EPOXY-(S10/S11/S12/S13/S14)	10	46	400
	PVC-DIST-(S10/S11/S12/S13/S14)	10	26	400

<sup>&</sup>quot;The number of molecules of each species is indicated, where each additive corresponds to an approximate 20% mass composition, which is often found in commercial PVC products.<sup>13</sup>

minimize fluctuations in the pressure tensor, values were averaged over 400 ps sub-blocks up to 5% strain. The error bars were calculated from a 95% confidence interval of 10 replicas of the system, and the average stress values were obtained. The Young's modulus values were obtained by calculating the slope of the linear region of the stress—strain curves. Additionally, the  $T_{\rm g}$  was determined, according to our previous work, <sup>36</sup> by subjecting the systems to a cooling process from 600 to 100 K at a rate of  $4 \times 10^{-3}$  K/ps (refer to Figure S1) and fitting the volume versus temperature plot to a regularization function <sup>46</sup> as shown below:

$$V(T) = aT + b - c(T - T_{\rm g}) \left[ 1 + \frac{(T - T_{\rm g})}{\sqrt{(T - T_{\rm g})^2 + \xi^2}} \right]$$
(2)

where  $\xi$  is the regularization parameter (where  $1 > \xi \gg 0$ ), and the parameters a, b, and c are obtained from fitting of the data to eq 2.

The enthalpy and volume of mixing ( $H^E$  and  $V^E$ ) different solvents with the PVC were calculated using eqs 3 and 4, respectively:

$$H^{\rm E} = H_{\rm m} - \sum x_i \langle H \rangle_i \tag{3}$$

$$V^{\rm E} = \langle V \rangle_{\rm m} - \sum x_i \langle V \rangle_i \tag{4}$$

where  $\langle H \rangle_{\rm m}$  and  $\langle V \rangle_{\rm m}$  represent the ensemble averages of the mixture's molar enthalpy and volume (here, a mole of PVC corresponds to a PVC<sub>120</sub> chain), respectively. The variables  $x_i$ ,  $\langle H \rangle_i$  and  $\langle V \rangle_i$  represent the mole fraction, enthalpy, and volume of *i*th compound in its pure liquid state and solute. The Flory–Huggins solution theory<sup>47</sup> was used to compute the Flory–Huggins parameter based on the enthalpy of mixing:

$$\chi_{12} = \frac{H^{\mathrm{E}}}{RTN_{1}\Phi_{2}} \tag{5}$$

where  $N_1$  is the number of solvent molecules, T is the temperature (K), R is the universal gas constant,  $\Phi_2$  is the lattice volume fraction  $\Phi_2 = \frac{xN_2}{N}$ ,  $N_2$  is the number of PVC<sub>120</sub> chains, each of which has x repeat units, and N is the total number of sites  $(N = N_1 + xN_2)$ .

The contact angle was calculated to evaluate the interfacial interaction of the bioderived solvents with PVC; the water contact angle was also calculated for reference. To do this, a planar surface was built using 40 molecules of PVC<sub>120</sub>, which was initially equilibrated in the semianisotropic NPT ensemble (in which only the z-dimension fluctuated). The same annealing procedure described above was applied. Next, a cylindrical liquid droplet (to avoid line tension effects<sup>48</sup>) was placed above the equilibrated PVC surface. Then, a second equilibration was run for 40 ns in the canonical ensemble (NVT), followed by a production run. Based on the sampled

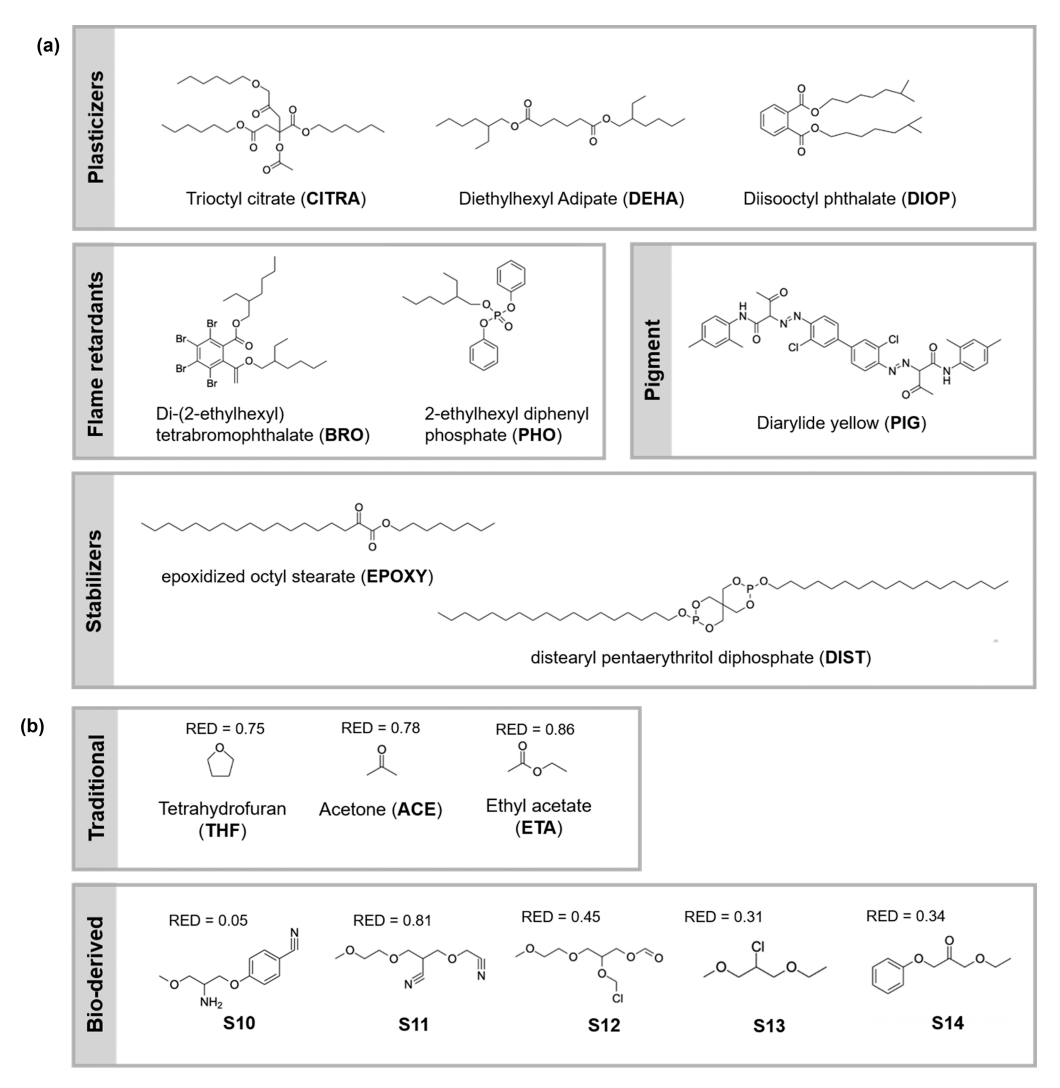


**Figure 2.** (a) Molecular structures of plasticizers, flame retardants, pigment, and stabilizers. (b) Molecular structures of traditional and bioderived solvents. RED: relative energy difference describing the compatibility between PVC and solvent based on their solubility parameters, obtained from literature. <sup>23,24</sup>

Table 2. Number of Solvent Molecules Corresponding to Different Simulated Concentrations Used to Investigate the Mixing Thermodynamics of PVC ( $10 \text{ PVC}_{120} \text{ Chains}$ ) in Solvents

Solvent mass concentration (%)	ACE	ETA	THF	S10	S11	S12	S13	S14
10	718	473	579	202	202	183	273	215
50	1292	852	1041	379	379	328	492	387
80	3229	2129	2601	821	946	820	1230	977

configurations, the yz density projection of the solvent molecules and the z-direction density profile of PVC<sub>120</sub> were calculated. In our approach, the surface point  $(z_p)$  of the PVC surface was defined as the point at which the density of the z-direction (perpendicular to the interface) profile corresponds to one-third of the bulk density. Similarly, the edge of the droplet was determined based on the bidimensional density projection using the same one-third criteria. Then, the edge points of the solvent droplet were used to fit the equation  $(z-z_0)^2+(y-y_0)^2=R^2$ , and the contact angle was obtained by calculating the slope of the fitted equation at  $z=z_p$ .

Finally, the optimized structures of the individual solvent molecules obtained from the DFT calculations described earlier were used to evaluate the general interaction property functions (GIPFs)<sup>49</sup> in the Multiwfn package.<sup>50</sup> These GIPF

values can be used as indicators for screening solvation performance, so they are included here to help rationalize the performance of the different bioderived solvents. The GIPF values were derived based on the electrostatic potential (ESP) using the van der Waals (vdW) surfaces. The electron density isosurface was set at 0.001 e/Bohr³,  $^{51}$  similar to our previous works.  $^{52-54}$  This method allowed us to compute parameters such as molecular volume  $(V_{\rm m})$ , molecular surface area (SA), maximum and minimum ESP values  $(V_{\rm min}$  and  $V_{\rm max})$ , average ESP value  $(\overline{V})$ , positive and negative ESP average values  $(\overline{V}^+$  and  $\overline{V}^-$ , respectively), total ESP variance  $(\sigma^2_{\rm tot})$ , molecular polarity index (MPI), and polar surface area (with ESP < 10 kcal/mol).

#### 3. RESULTS AND DISCUSSION

**3.1.** Effects of Additives on the PVC Structure. As mentioned above, plasticizers are commonly used to enhance the flexibility of PVC. Their primary function, derived from their molecular architecture, is to weaken the intermolecular interactions among neighboring PVC segments, facilitating the ease with which polymer chains slide past one another. As expected, our simulations indicate that the plasticizers tend to decrease the calculated  $T_{\rm g}$  values of pure PVC (Table 3), with

Table 3. Effect of Different Plasticizers on the Calculated  $T_{\rm g}$  Value of PVC<sup>a</sup>

System	Simulated $T_{\rm g}$ (K)	Experimental $T_{\rm g}$ (K)	Plasticizer content (% w/w)
PVC	366	$350 - 370^{56 - 59}$	_
PVC-CITRA	328	307 <sup>60</sup>	33
PVC-DEHA	325	$228 - 301^{61 - 64}$	10-20
PVC-DIOP	341	$260 - 330^{65,66}$	20-50

<sup>a</sup>The plasticizer content corresponds to the % w/w used to determine the experimental  $T_{\rm g}$  range. Refer to Figure S1 for the volume—temperature plots used to obtain the  $T_{\rm g}$  values. The simulated  $T_{\rm g}$  for pure PVC was obtained from our previous work. <sup>36</sup>

the following trend: CITRA < DEHA < DIOP (similar  $T_{\rm g}$  values are obtained for CITRA and DEHA), similar to

simulation results by Li et al.  $^{17}$  and experimental data presented in Table 3. Discrepancies between our predictions and experimental results might originate from inherent differences in methodology (e.g., cooling rates), as highlighted by Mohammadi et al.  $^{55}$  The reduced  $T_{\rm g}$  values indicate enhanced segmental mobility within the polymer chains in the presence of these additives.

The coordination between the additives and the PVC sites can be observed in further detail by examining the RDF analyses for representative additives of each group (plasticizers, flame retardants, pigments, and stabilizers) presented in Figure 3, while the other plots can be found in Figure S2. As observed in Figure 3a and Figure S2a and b, the double-bonded oxygen sites (Od) of the plasticizers display varying degrees of coordination with the PVC atoms. Notably, all of the plasticizers exhibit short-range interactions between the Od and H sites at a distance around 0.25 nm. The coordination of the Od sites with the C sites of PVC shows two peaks around 0.35 and 0.45 nm, suggesting a bidentate configuration among these sites. The coordination between the oxygen in the alkyl chains of the plasticizers (Oc) and the PVC sites is presented in Figure S2e-g; the plots exhibit very weak features. Smooth RDF profiles are obtained in Figure S2e, with a small Cl-Oc peak around 0.5 nm, and similar behavior is observed in Figure S3f and g. Slightly higher C-Oc peaks (but at an extended

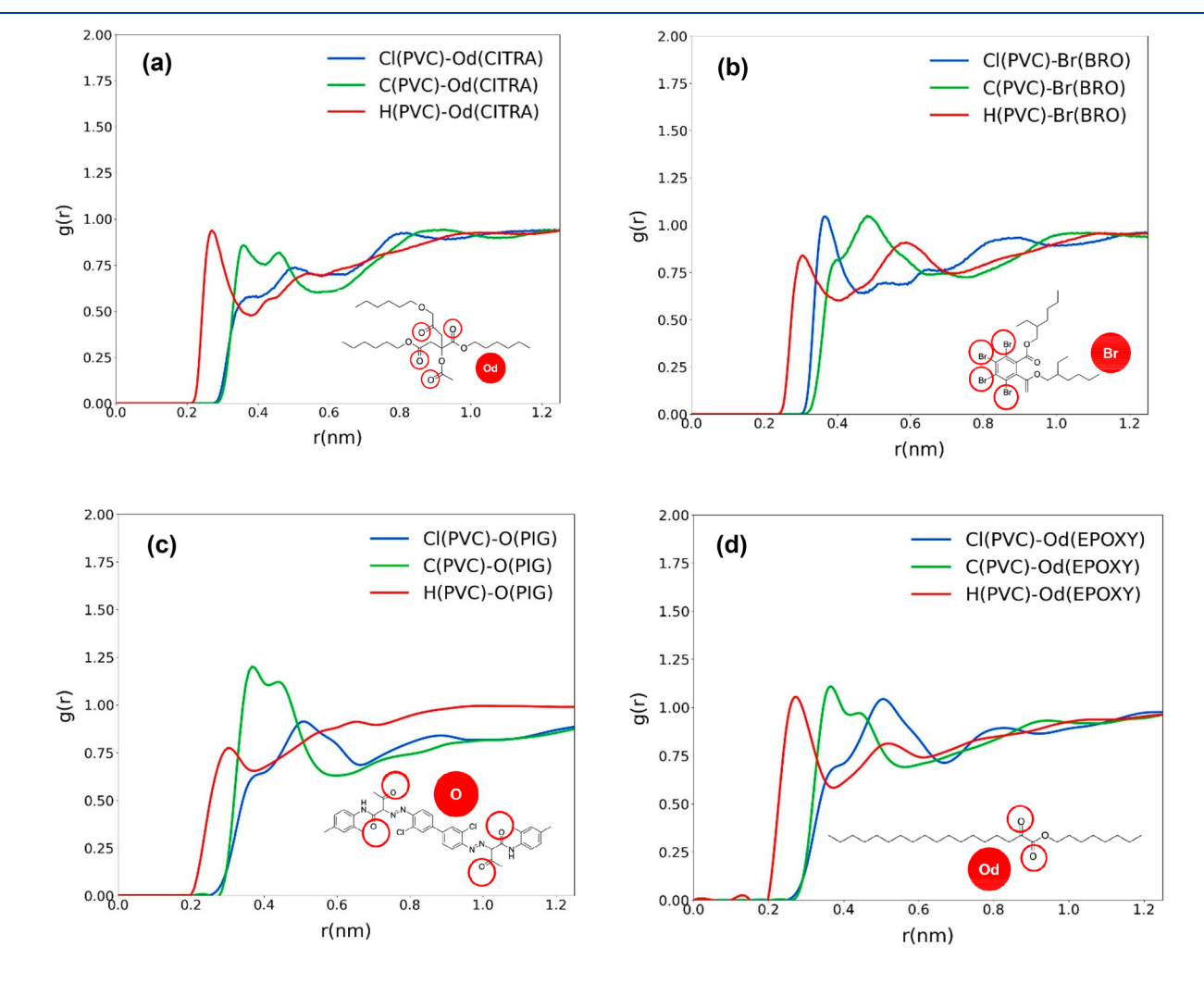


Figure 3. Site-site RDFs of PVC + additive systems: (a) PVC-CITRA, (b) PVC-BRO, (c) PVC-PIG, and (d) PVC-EPOXY.

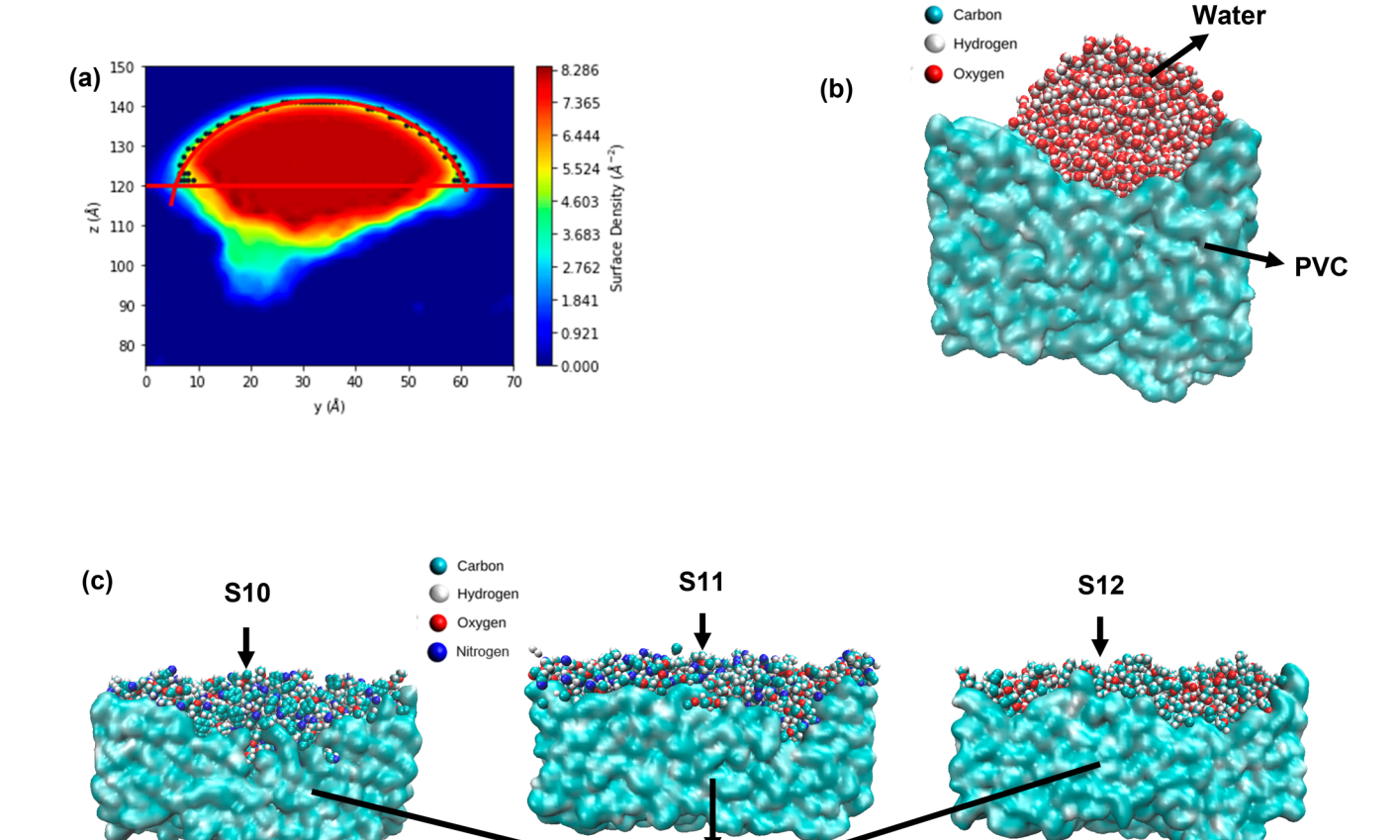


Figure 4. (a) Projection of the water droplet density along the yz plane and representative snapshots of the (b) water and (c) S10, S11, and S12 droplets on the PVC surface.

**PVC** 

distance of 0.55 nm) are obtained for DEHA and DIOP, compared with CITRA.

Considering flame retardants, pigment, and stabilizers, Figure 3b-d and Figure S2c and d show the interaction between PVC and BRO, PIG, EPOXY, PHO, and DIST, respectively. For instance, the bromine atoms in the BRO system (Figure 3b) show short-range interactions around 0.30 nm with the H sites of PVC, which could be attributed to electrostatic interactions and the size of the bromine atoms. Similar behavior is also observed for the P site of PHO in Figure S2c, which exhibits an H(PVC)-P(PHO) peak around 0.35 nm as well as C(PVC)-P(PHO) beyond the first peak. Similar features are also observed in the RDFs presented in Figure 3c and d and Figure S2d. On the other hand, the interaction between Cl(PVC) and P(PHO) appears notably weaker than that between Cl(PVC) and Br(BRO). This can probably be attributed to steric hindrance effects given that the P site in PHO is obscured by its O sites. The prominent first peak observed with Cl and Br might suggest a volume exclusion effect.

Generally, we observe similar trends of the H sites of PVC primarily interacting with the additive sites around 0.25–0.35 nm, followed by the Cl and C sites. However, there are some stark differences, such as an unusually strong Cl peak in Figure 3b.

**3.2. Solvation Analyses.** Beyond the static representations of the site—site interactions between PVC and different additives, it is essential to investigate the molecular impacts of

solvating PVC (and its additives) in different solvent environments. The primary performance benchmark for our analyses of the bioderived solvents is the commonly used solvent THF. As a first step, we attempt to calculate the contact angles of some of the evaluated bioderived solvents on a PVC surface (with no additives); the contact angle of water on the PVC surface is also calculated to evaluate the reliability of our approach. Figure 4a shows the density projection of the water droplet (Figure 4b), the fitted surface (red line), the points used to fit the surface (black points), and the PVC delimiting surface (horizontal red line). Accordingly, we calculate a contact angle of 74.58° for the water droplet at a temperature of 298 K, which is close to the experimental value obtained in the literature  $(82 \pm 2^{\circ})^{.67}$  We used the same approach to predict the contact angles of solvents S10, S11, and S12. However, the visual snapshots (Figure 4c) indicate that solvents S10, S11, and S12 are not able to maintain a droplet structure, due to their strong wetting/solvation interactions with the PVC, which is consistent with predictions from the previous DFT calculations.<sup>23</sup> To help qualitatively depict the solvation further, visual analyses in Figure 5 corresponding to the bulk systems (PVC-solvent) presented in Table 1 highlight that in the presence of these solvents, PVC molecules no longer cluster but disentangle from one another, emphasizing the strength of these solvents.

The RDFs offer additional insight into the molecular interactions between PVC and these solvents. However, it is important to note that these are not homogeneous systems

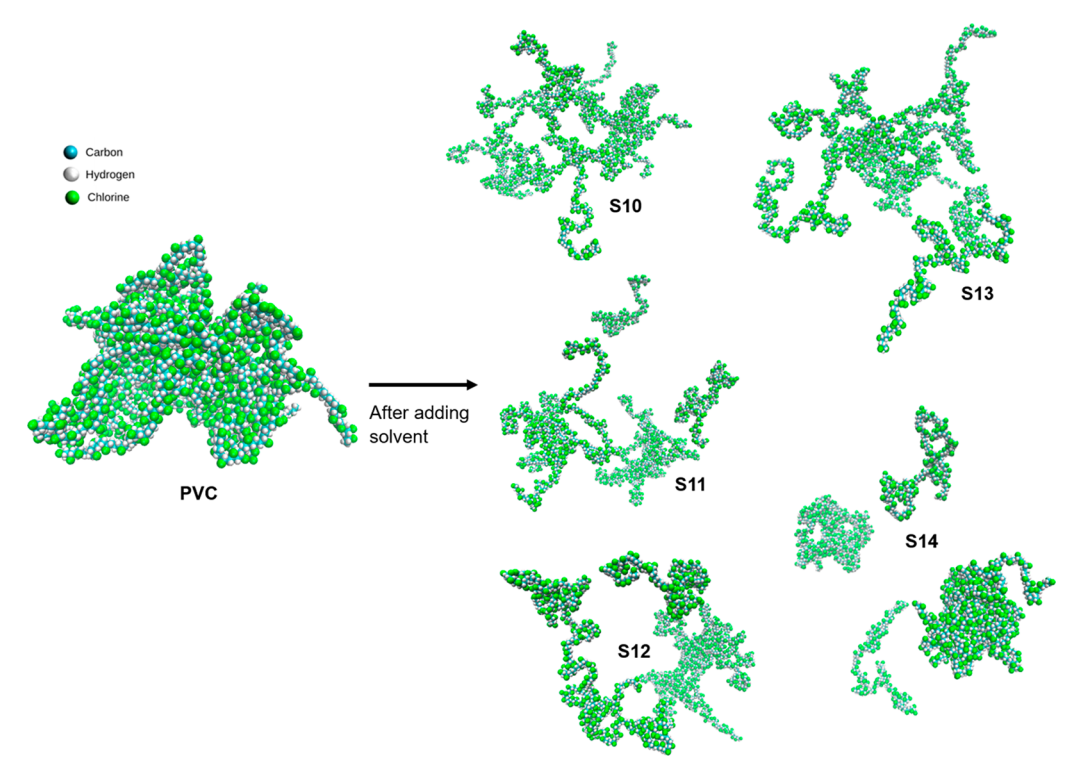


**Figure 5.** Visual analysis of PVC chain disentanglement in S10, S11, S12, S13, and S14 solvents (snapshots from MD trajectories; solvent molecules removed for visual clarity). Refer to Table 1 for the compositions of the PVC–solvent systems. The snapshot at the left represents PVC at t = 0, prior to solvation.

(e.g., due to clustering), and as such, the RDF peak heights may be skewed due to the default bulk normalization factor. Nonetheless, the RDFs for the PVC-solvent systems in Figure 6 show several pronounced peaks indicative of specific molecular interactions. For solvents S10 and S11, a marked interaction is observed between the H sites of PVC and the Nt sites, exemplified by a short-range peak around 0.27 nm (Figure 6a and b). This interaction is less pronounced with the Oc sites, indicated by a g(r) value significantly lower ( $\sim$ 0.25) at the same distance. In solvents S13 and S14, the H sites of PVC primarily interact with the Cl (Figure 6d) and Od sites (Figure 6e), respectively. In contrast, S12 showcases subdued interactions with significantly diminished g(r) values (Figure 6c and Figure S3e). Another unique feature is the dual-peaked coordination between the C sites of PVC and Nt sites of S10 (Figure S3a) and S11 (Figure S3c), located around 0.35 and 0.45 nm. In the S13 solvent, we observe a similar bidentate coordination between the C sites of PVC and Cl sites (Figure S3g); for S12 and S14, this feature is found between C sites of PVC and Od sites (Figure S3e and i). Coordination profiles between Cl of PVC and the respective solvent sites can be found in Figure S3b, d, f, h, and j.

When evaluating the THF RDF (as a comparison), we also observe a bidentate coordination between C of PVC and the Oc of THF (Figure S3k). Notably, H of PVC and Oc of THF display a distinct first peak at around 0.25 nm (Figure 6f). Overall, the Nt site stands out as the predominant interaction site for solvents S10 and S11 with PVC. For S13, the Cl site takes precedence, and for S12 and S14, it is the Od site. In the case of THF, it is the Oc site. The comparison of these coordination profiles with THF could suggest potential similar solvation mechanisms. The next step is to explore how these solvents influence interactions between PVC and its additives.

Figure S4 shows the RDFs for the PVC-CITRA-solvent systems. As seen in Figure S4a, there is a change when S10 is introduced to the PVC system in the presence of CITRA. In the pure PVC-CITRA system (Figure 3a), the C(PVC)-Od(CITRA) RDF shows a first peak intensity of approximately 0.8. However, this peak decreases drastically to about 0.25 in the PVC-CITRA-S10 system (Figure S4a). Additionally, the PVC-CITRA-S12 system (Figure S4c) and PVC-CITRA-S14 system (Figure S4e) reflect this same decrease in g(r)values, to around 0.6 and 0.4, respectively. Contrarily, both the PVC-CITRA-S11 (Figure S4b) and PVC-CITRA-S13 systems retain relatively consistent g(r) values. By comparison of the C(PVC)-Nt(S10) RDF in both the PVC-S10 (Figure S3a) and PVC-CITRA-S10 (Figure S4a) systems, a slight increase in the g(r) value is observed. This indicates that as PVC's interactions with CITRA become weaker, its coordination with the solvent intensifies. Conversely, the C(PVC)-Od(S14) RDF displays a diminished g(r) when the solvent is incorporated, as shown in Figure S4e.

Exploring other plasticizers (DEHA and DIOP) offers additional insights. Comparing the C(PVC)–Od(CITRA) RDF of PVC–CITRA–S10 (Figure S4a) to PVC–DEHA–S10 (Figure S5a) and PVC–DIOP–S10 (Figure S6a) shows a more pronounced first peak intensity in the latter systems. This implies that C in PVC has a weaker affinity with CITRA than with DIOP and DEHA when immersed in the S10 solvent. Moreover, the systems with S11 (Figures S5b and S6b), S12 (Figures S5c and S6c), S13 (Figures S5d and S6d), and S14 (Figures S5e and S6e) solvents display varying g(r) values upon solvent addition. Such findings suggest that specific plasticizers might dissociate from the PVC matrix more easily than others in these solvents (refer to Table 4).

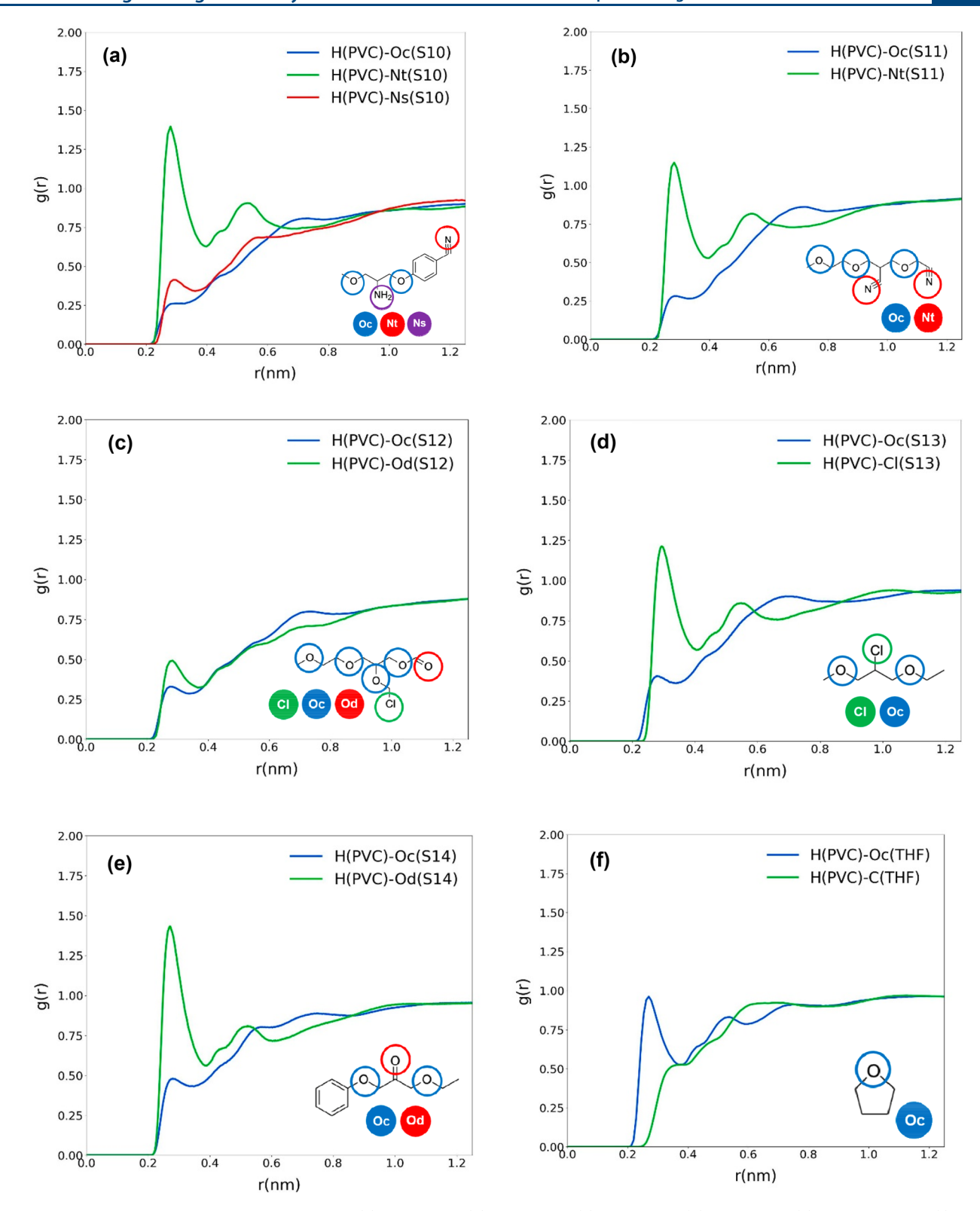


Figure 6. Site-site RDFs of PVC-solvent systems: (a) PVC-S10, (b) PVC-S11, (c) PVC-S12, (d) PVC-S13, (e) PVC-S14, and (f) PVC-THF.

In relation to flame retardants, the C(PVC)-Br(BRO) peaks show reduced g(r) values in S10 (Figure S7a), S13 (Figure S7d), and S14 (Figure S7e). In contrast, increased g(r) values are seen in parts S11 (Figure S7b) and S12 (Figure S7c). For the C(PVC)-P(PHO) peaks, there is an increase in all solvents except in S10 and S11 (Figure S8). Regarding

stabilizers, the C(PVC)—Od(EPOXY) RDF peak shows reductions in S11 and S13 (Figure S10b and d), while the C(PVC)—P(DIST) peaks are reduced in S10, S11, and S12 (Figure S11a—c). For the pigment PIG, the C(PVC)—O(PIG) RDF peak decreases in S10 (Figure S9a) and S11 (Figure S9b) but increases in S12 (Figure S9c) and S13 (Figure S9d). In the

Table 4. Summary of the Solvent Performance Based on the g(r) Value of RDFs of Respective Systems (Figures S4-S11)<sup>a</sup>

	C(PVC)- Od(CITRA)	C(PVC)- Od(DEHA)	C(PVC)- Od(DIOP)	C(PVC)- Br(BRO)	C(PVC)- P(PHO)	C(PVC)- O(PIG)	C(PVC)- Od(EPOXY)	C(PVC)- O(DIST)
S10	d	d	i	d	d	d	i	d
S11	i	d	i	i	d	d	d	d
S12	d	i	i	i	i	i	i	d
S13	i	i	i	d	i	i	d	i
S14	d	d	i	d	i	d	i	i

""d" implies that the g(r) value decreases, while "i" implies that the g(r) value increases, relative to the PVC + additive system without solvent (Figure 3).

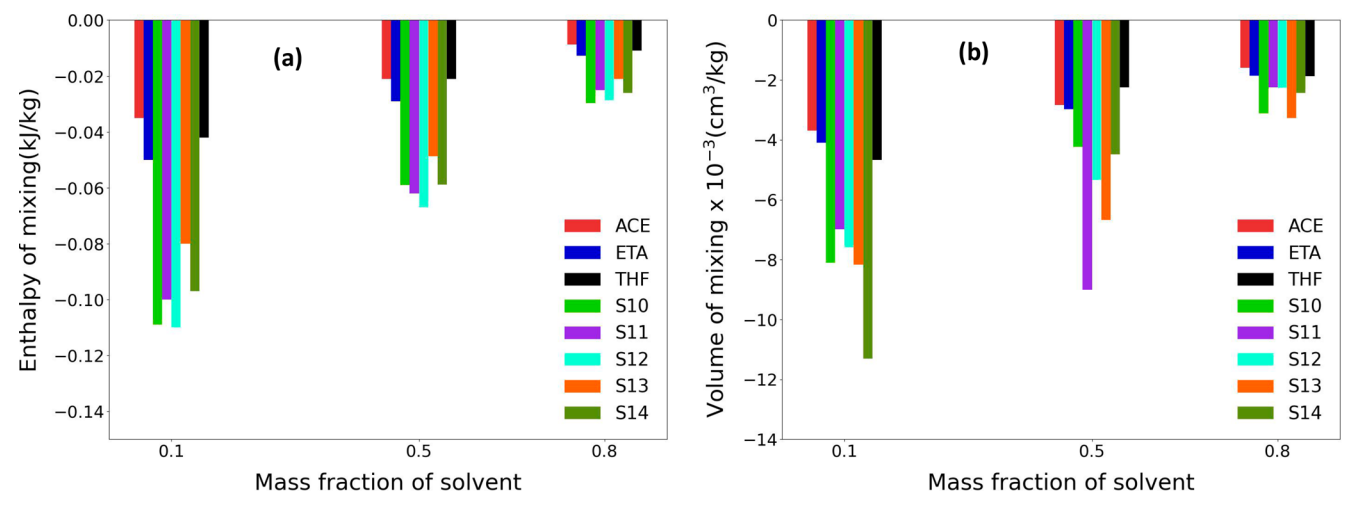


Figure 7.  $H^{E}$  and  $V^{E}$  values of PVC in ACE, ETA, S10, S11, S12, and THF at varying solvent concentrations (0.1, 0.5, and 0.8 mass fractions) at 300 K.

S14 solvent (Figure S9e), the peak shifts to a larger distance of 0.5 nm with reduced intensity.

Table 4 presents the qualitative solvent performance in these systems, as determined by the RDF, highlighting whether the solvent increases or diminishes the interaction strength between PVC and the associated additives. The observations indicate that S10, S11, and S14 reduce the interactions between PVC and most of the additives examined, suggesting they are likely the most effective PVC solvents among the bioderived options.

We further analyze these findings by benchmarking the bioderived solvent performance against THF. Table S1 summarizes the predicted  $R_g$  and SA values of PVC in the previously mentioned solvents when the specified additives are introduced into the system. For PVC dissolved in THF, the  $R_{\alpha}$ values across different additives ranged from 1.99 nm (observed with CITRA) to 4.13 nm (observed with DIST). Most of the SA values of PVC in THF fall within 700-800 nm<sup>2</sup>, with an average of 761.2 nm<sup>2</sup>. In comparison, the average PVC  $R_g$  in S10 (2.38 nm) and S14 (2.32 nm) indicates similar expanded PVC configurations, corroborated by SA values averaging 700.2 nm<sup>2</sup> in S10 and 702.31 nm<sup>2</sup> in S14. PVC has the least expanded structure in S12, reflected by an average  $R_{\sigma}$ of 2.19 nm and an SA of 626.2 nm<sup>2</sup>. This is not surprising, as it appears to have the weakest interactions with PVC, as discussed previously (refer to Figure 6c and Figure S3e).

Overall, S10 and S14 most effectively expand the PVC structure among the bioderived solvents. Their efficiency closely mirrors that of THF, achieving approximately 92% of the PVC  $R_{\rm g}$  and SA values exhibited in THF. While THF still registers higher  $R_{\rm g}$  and SA values, the metrics from S10 and

S14 are reasonably close, suggesting that these bioderived solvents may be effective compounds, nearly matching the performance of THF in influencing the PVC structure.

3.3. Mixing Thermodynamics and Mechanical Behavior. Figure 7 presents the excess enthalpy  $(H^{E})$  of mixing and the excess volume  $(V^{E})$  of mixing values of PVC with the solvents shown in Figure 2 at different solvent mass fractions (0.1, 0.5, 0.8). The  $H^{E}$  value provides an average indication of the PVC-solvent interaction energetics relative to an ideal mixture, with a more negative enthalpy, suggesting stronger, favorable interactions. Concurrently, the  $V^{E}$  value measures the average volume change upon mixing, with values of lower magnitude indicating smaller deviations from an ideal mixture (i.e., less swelling/contraction). As mentioned earlier, studies of PVC-additive mixtures (especially in solvents) are relatively rare. While there are some data in the literature relevant to PVC-additive mixtures, the available experimental data for  $H^{E}$ and  $V^{\rm E}$  correspond to PVC blends,  $^{68-73}$  thus compromising direct comparisons to our calculations. Nonetheless, the available experimental data fall within the same order-ofmagnitude as our predicted values.

According to Figure 7, the bioderived solvents exhibit large negative enthalpy values when present at all mass fractions, while ACE and THF tend to have the smallest (least negative)  $H^{\rm E}$  values overall, indicating "weaker" PVC interactions. As the solvent concentration increases, the  $H^{\rm E}$  values tend toward zero, suggesting diminishing nonideality, as PVC becomes more dilute.

On the other hand, the  $H^{\rm E}$  and  $V^{\rm E}$  values of the bioderived solvents appear to be approximately twice that of the traditional solvents, a trend that might relate to the RED

values shown in Figure 2. The bioderived solvents, which exhibit more negative  $H^{\rm E}$  values with PVC, may provide some performance advantages. Furthermore, based on the Flory–Huggins interaction parameters presented in Table S2, the bioderived solvents show more negative values across all mass fractions (compared to traditional solvents), highlighting stronger favorable interactions with PVC. The  $V^{\rm E}$  data, shown in Figure 7b, indicate that bioderived solvents have more negative  $V^{\rm E}$  values at 80% solvent concentration compared to traditional solvents. Among the bioderived solvents, S10 has the most negative  $H^{\rm E}$ , followed by S12 and S14. S11 and S12 exhibit the least negative  $V^{\rm E}$ , followed by S14 and S10. In traditional solvents, ACE and THF tend to yield the most ideal mixing behavior at different concentrations.

Figure 8 shows the Young's modulus values of PVC, as obtained from the stress-strain profiles (see Figure S12),

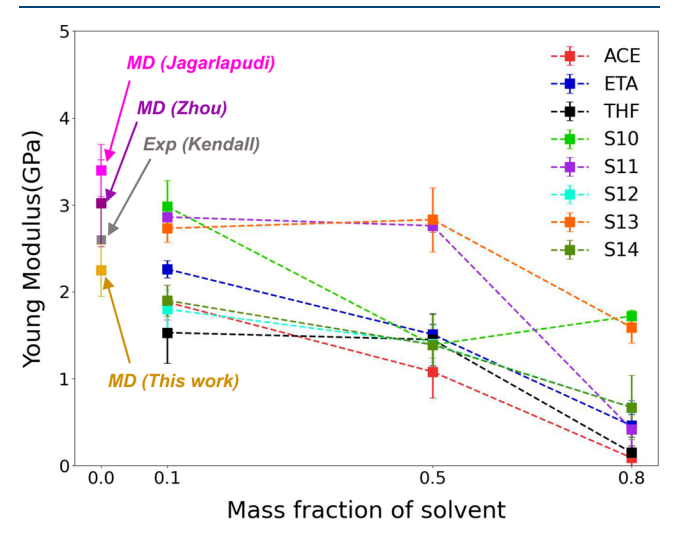


**Figure 8.** Young's modulus of PVC at different solvent concentrations (at 300 K). As a benchmark, we compare our value of pure PVC (at 0% solvent concentration) with experimental data from Kendall and Siviour<sup>74</sup> and MD results by Zhou et al.<sup>75</sup> and Jagarlapudi et al.<sup>18</sup>

corresponding to the aforementioned solvent fractions. We also compare our simulation results to experimental data<sup>74</sup> and other MD simulations<sup>18,75</sup> at 0% solvent concentration; predicted values are in reasonable agreement with existing results. S10 retains the highest Young's modulus at both 10% and 80% solvent concentrations, indicating its tendency to

increase the stiffness of the material, which is generally consistent with the  $H^{E}$  and  $V^{E}$  values (stronger interactions in the mixture and more volume contraction). In contrast, ACE and THF show the lowest Young's moduli at 80% solvent concentration, highlighting the mechanical destabilizing effects of these traditional solvents on PVC's structural rigidity. These observations are further corroborated upon inspection of the stress-strain curves in Figure S12. ACE, ETA, and THF show a pronounced change in PVC's stress-strain behavior at elevated solvent concentrations (especially from 50% to 80% solvent concentration). Such shifts can be correlated to these solvents reducing the PVC chain's volumetric density more significantly than the bioderived solvents. Among the bioderived solvents, S11, S12, and S14 show the lowest Young's modulus values at 80% solvent concentration. Table 5 summarizes the absolute values of these properties, providing a perspective on the solvent performance.

Based on the structural and thermomechanical metrics evaluated, S10, S11, and S14 are predicted to be effective at separating additives from PVC. Table S3 presents the GIPF properties of these solvents, which can help to suggest possible ESP-based origins of the solvent performance. Compared to the traditional solvents, these bioderived alternatives predominantly exhibit larger  $V_m$  and SA values. Their other GIPF values present some variations. For instance, S11 has a strongly polar character due to its high  $\overline{V}^-$ ,  $\overline{V}^+$ , and MPI. In contrast, S10 and S12 have more extreme ESP values, which could affect their PVC interactions. Notably, S10s highly negative  $V_{\min}$ suggests the origin of its robust attractive interactions, whereas S12's elevated  $V_{\text{max}}$  hints at stronger repulsive interactions, as further evidenced by Figure 6c and Figure S3e, which highlight the weak interactions between S12 and PVC. S10 corresponds to the highest  $\sigma_{\text{tot}}^2$  value, signifying the most nonuniform ESP distribution. Traditional solvents such as ACE and THF also rank high in this context. These ESP attributes among bioderived solvents might be linked to the observed favorable enthalpic interactions (see Figure 7).

# 4. FINAL REMARKS

In this study, we used molecular simulations to assess the performance of five bioderived solvents compared to traditional industrial solvent options (e.g., ACE, THF, and ETA) with respect to PVC solvation performance in the presence of different commonly used additives. We quantified the effects of these additives on PVC, as well as an analysis of the solvation

Table 5. Summary of the Relative Solvent Performance Based on the Enthalpy of Mixing, Volume of Mixing, and Young's Modulus at 0.1, 0.5, and 0.8 Solvent Mass Fractions<sup>a</sup>

Highest to lowest magnitude (absolute) $\rightarrow$									
Enthalpy of mixing	0.1	S10	S12	S11	S14	S13	ETA	THF	ACE
	0.5	S12	S11	S10	S14	S13	ETA	THF	ACE
	0.8	S10	S12	S14	S11	S13	ETA	THF	ACE
Volume of mixing	0.1	S14	S13	S10	S12	S11	THF	ETA	ACE
	0.5	S11	S13	S12	S14	S10	ETA	ACE	THF
	0.8	S13	S10	S14	S11	S12	ETA	THF	ACE
Young's modulus	0.1	S10	S11	S13	ETA	S14	ACE	S12	THF
	0.5	S13	S11	ETA	THF	S10	S12	S14	ACE
	0.8	S10	S13	S12	S14	ETA	S11	THF	ACE

<sup>&</sup>lt;sup>a</sup>The right arrow shows the ranking of the solvent based on the magnitude of its respective absolute values.

of PVC and its additives in the selected bioderived solvents versus THF. Subsequently, we investigated the mixing thermodynamics and evaluated the mechanical impacts of these solvents on PVC. Although experimental data to validate our predictions was sparse, we observed good agreement where comparisons were possible.

Structurally, these bioderived solvents induce expanded PVC configurations comparable to THF, as evidenced by  $R_{\rm g}$  and SA values. The bioderived solvents also diminish the interactions between PVC and most of its additives, as seen from the RDFs. From a thermodynamic perspective, they exhibit more favorable enthalpic interactions, while more negative  $V^{\rm E}$  values might indicate a tendency for PVC to contract. In comparison, PVC appears to have greater mechanical rigidity in bioderived solvents, which might not be conducive for structural disruption. The GIPF data hint at the origin of bioderived solvent performance, which is consistent with the larger  $H^{\rm E}$  values.

While THF remains a prominent solvent for PVC-additive separation, bioderived solvents may parallel or even exceed its performance. This makes them promising substitutes, especially given the sustainability concerns. As the next stage of evaluation, experimental validation and practical assessments are needed, such as cost, ease of synthesis, and toxicity.

## ASSOCIATED CONTENT

#### **Data Availability Statement**

The data sets generated during and/or analyzed during the current study are available from the corresponding author on reasonable request.

## **Solution** Supporting Information

The Supporting Information is available free of charge at https://pubs.acs.org/doi/10.1021/acs.iecr.3c03809.

Volume–temperature plots to obtain  $T_{\rm g}$ ; site-to-site RDFs for PVC–additive, PVC–solvent, and PVC–additive–solvent systems; stress–strain profiles;  $R_{\rm g}$  and SA of PVC in PVC–additive–solvent systems; Flory–Huggins parameters of PVC in respective solvents; and GIPF properties of isolated solvent molecules. (PDF)

## AUTHOR INFORMATION

# **Corresponding Author**

C. Heath Turner — Department of Chemical and Biological Engineering, The University of Alabama, Tuscaloosa, Alabama 35487-0203, United States; oorcid.org/0000-0002-5707-9480; Phone: 205-348-1733; Email: hturner@eng.ua.edu

### **Authors**

Feranmi V. Olowookere – Department of Chemical and Biological Engineering, The University of Alabama, Tuscaloosa, Alabama 35487-0203, United States

Gabriel D. Barbosa – Department of Chemical and Biological Engineering, The University of Alabama, Tuscaloosa, Alabama 35487-0203, United States

Complete contact information is available at: https://pubs.acs.org/10.1021/acs.iecr.3c03809

#### Notes

The authors declare no competing financial interest.

#### ACKNOWLEDGMENTS

This work is supported by the National Science Foundation (Award Nos. 2132133 and 2029387). We are grateful to the Alabama Supercomputer Authority for computational support.

#### REFERENCES

- (1) Shamsuyeva, M.; Endres, H.-J. Plastics in the context of the circular economy and sustainable plastics recycling: Comprehensive review on research development, standardization and market. *Compos. Part C* **2021**, *6*, 100168.
- (2) Mijangos, C.; Calafel, I.; Santamaría, A. Poly (vinyl chloride), a historical polymer still evolving. *Polymer* **2023**, *266*, 125610.
- (3) Norfarhana, A.; Ilyas, R.; Ngadi, N.; Sharma, S.; Sayed, M. M.; El-Shafay, A.; Nordin, A. Natural Fiber-Reinforced Thermoplastic ENR/PVC Composites as Potential Membrane Technology in Industrial Wastewater Treatment: A Review. *Polymers* **2022**, *14* (12), 2432.
- (4) Rahman, M.; Brazel, C. S. The plasticizer market: an assessment of traditional plasticizers and research trends to meet new challenges. *Prog. Polym. Sci.* **2004**, *29* (12), 1223–1248.
- (5) Babinsky, R. PVC additives: A global review. *Plastics, Additives and Compounding* **2006**, 8 (1), 38-40.
- (6) Wojnowska-Baryła, I.; Bernat, K.; Zaborowska, M. Plastic waste degradation in landfill conditions: the problem with microplastics, and their direct and indirect environmental effects. *Int. J. Environ. Res. Public Health* **2022**, *19* (20), 13223.
- (7) Boyle, D.; Catarino, A. I.; Clark, N. J.; Henry, T. B. Polyvinyl chloride (PVC) plastic fragments release Pb additives that are bioavailable in zebrafish. *Environ. Pollut.* **2020**, 263, 114422.
- (8) Xu, S.; Yu, Y.; Qin, Z.; Wang, C.; Hu, Q.; Jin, Y. Effects of 2-ethylhexyl diphenyl phosphate exposure on the glucolipid metabolism and cardiac developmental toxicity in larval zebrafish based on transcriptomic analysis. Comp. Biochem. Physiol., Part C: Toxicol. Pharmacol. 2023, 267, 109578.
- (9) Nurlatifah; Yamauchi, T.; Nakajima, R.; Tsuchiya, M.; Yabuki, A.; Kitahashi, T.; Nagano, Y.; Isobe, N.; Nakata, H. Plastic additives in deep-sea debris collected from the western North Pacific and estimation for their environmental loads. *Sci. Total Environ.* **2021**, 768, 144537.
- (10) Brennecke, D.; Duarte, B.; Paiva, F.; Caçador, I.; Canning-Clode, J. Microplastics as vector for heavy metal contamination from the marine environment. *Estuarine, Coastal and Shelf Sci.* **2016**, *178*, 189–195.
- (11) Karimi Estahbanati, M. R.; Kong, X. Y.; Eslami, A.; Soo, H. S. Current developments in the chemical upcycling of waste plastics using alternative energy sources. *ChemSusChem* **2021**, *14* (19), 4152–4166.
- (12) Hsissou, R.; Seghiri, R.; Benzekri, Z.; Hilali, M.; Rafik, M.; Elharfi, A. Polymer composite materials: A comprehensive review. *Compos. Struct.* **2021**, 262, 113640.
- (13) Li, D.; Panchal, K.; Vasudevan, N. K.; Mafi, R.; Xi, L. Effects of molecular design parameters on plasticizer performance in poly (vinyl chloride): A comprehensive molecular simulation study. *Chem. Eng. Sci.* **2022**, 249, 117334.
- (14) Yang, F.; Hlavacek, V. Improvement of PVC wearability by addition of additives. *Powder Technol.* **1999**, *103* (2), 182–188.
- (15) Demir, H.; Sipahioğlu, M.; Balköse, D.; Ülkü, S. Effect of additives on flexible PVC foam formation. *J. Mater. Process. Technol.* **2008**, *195* (1–3), 144–153.
- (16) Christie, R.; Abel, A. Disazo (Bishydrazone) pigments based on acetoacetanilides. *Phys. Sci. Rev.* **2021**, *6* (12), 791–805.
- (17) Li, D.; Panchal, K.; Mafi, R.; Xi, L. An atomistic evaluation of the compatibility and plasticization efficacy of phthalates in poly (vinyl chloride). *Macromolecules* **2018**, *51* (18), 6997–7012.
- (18) Jagarlapudi, S. S.; Cross, H. S.; Das, T.; Goddard, W. A., III Thermomechanical Properties of Nontoxic Plasticizers for Polyvinyl Chloride Predicted from Molecular Dynamics Simulations. *ACS Appl. Mater. Interfaces* **2023**, *15* (20), 24858–24867.

- (19) Özeren, H.s.D.; Balçık, M.; Ahunbay, M.G.k.; Elliott, J. R. In silico screening of green plasticizers for poly (vinyl chloride). *Macromolecules* **2019**, 52 (6), 2421–2430.
- (20) Leal-Duaso, A.; Pérez, P.; Mayoral, J. A.; García, J. I.; Pires, E. Glycerol-derived solvents: synthesis and properties of symmetric glyceryl diethers. ACS Sustainable Chem. Eng. 2019, 7 (15), 13004–13014.
- (21) Windels, S.; Diefenhardt, T.; Jain, N.; Marquez, C.; Bals, S.; Schlummer, M.; De Vos, D. E. Catalytic upcycling of PVC wastederived phthalate esters into safe, hydrogenated plasticizers. *Green Chem.* **2022**, 24 (2), 754–766.
- (22) Chen, X.; Wang, Y.; Zhang, L. Recent progress in the chemical upcycling of plastic wastes. *ChemSusChem* **2021**, *14* (19), 4137–4151.
- (23) Soyemi, A.; Szilvási, T. Calculated Physicochemical Properties of Glycerol-Derived Solvents to Drive Plastic Waste Recycling. *Ind. Eng. Chem. Res.* **2023**, *62* (15), 6322–6337.
- (24) Chatterjee, S.; Qian, S.; Soyemi, A.; Szilvási, T.; Bara, J. E. Synthesis and Properties of 2-Halo-1,3-diether-propanes: Diversifying the Range of Functionality in Glycerol-Derived Compounds. *Ind. Eng. Chem. Res.* **2023**, 62 (6), 2959–2967.
- (25) Hansen, C. M. Hansen Solubility Parameters: A User's Handbook; CRC Press: Boca Raton, FL, USA, 2007.
- (26) Hansen, C. M. Polymer additives and solubility parameters. *Prog. Org. Coat.* **2004**, *51* (2), 109–112.
- (27) Jorgensen, W. L.; Maxwell, D. S.; Tirado-Rives, J. Development and Testing of the OPLS All-Atom Force Field on Conformational Energetics and Properties of Organic Liquids. *J. Am. Chem. Soc.* **1996**, 118 (45), 11225–11236.
- (28) Valatin, J. Generalized hartree-fock method. Phys. Rev. 1961, 122 (4), 1012.
- (29) Yabe, M.; Mori, K.; Ueda, K.; Takeda, M. Development of PolyParGen Software to facilitate the determination of molecular dynamics simulation parameters for polymers. *J. Comput. Chem., Jpn.* **2019**, *5*, 2018-0034.
- (30) Dodda, L. S.; Vilseck, J. Z.; Cutrona, K. J.; Jorgensen, W. L. Evaluation of CM5 Charges for Nonaqueous Condensed-Phase Modeling. *J. Chem. Theory Comput.* **2015**, *11* (9), 4273–4282.
- (31) Tirado-Rives, J.; Jorgensen, W. L. Performance of B3LYP density functional methods for a large set of organic molecules. *J. Chem. Theory Comput.* **2008**, *4* (2), 297–306.
- (32) Ratcliff, L. E.; Mohr, S.; Huhs, G.; Deutsch, T.; Masella, M.; Genovese, L. Challenges in large scale quantum mechanical calculations. *Wiley Interdiscip. Rev.: Comput. Mol. Sci.* **2017**, 7 (1), No. e1290.
- (33) Yu, J.-S. K.; Chen; Yu, C.-H. Time-dependent density functional study of electroluminescent polymers. *J. Phys. Chem. A* **2003**, *107* (21), 4268–4275.
- (34) Jensen, F. Introduction to Computational Chemistry; John Wiley & Sons, 2017; pp 211–213.
- (35) Frisch, M. J.; Trucks, G. W.; Schlegel, H. B.; Scuseria, G. E.; Robb, M. A.; Cheeseman, J. R.; Scalmani, G.; Barone, V.; Mennucci, B.; Petersson, G. A.; Nakatsuji, H.; Caricato, M.; Li, X.; Hratchian, H. P.; Izmaylov, A. F.; Bloino, J.; Zheng, G.; Sonnenberg, J. L.; Hada, M.; Ehara, M.; Toyota, K.; Fukuda, R.; Hasegawa, J.; Ishida, M.; Nakajima, T.; Honda, Y.; Kitao, O.; Nakai, H.; Vreven, T.; Montgomery, J. A., Jr.; Peralta, P. E.; Ogliaro, F.; Bearpark, M.; Heyd, J. J.; Brothers, E.; Kudin, K. N.; Staroverov, V. N.; Kobayashi, R.; Normand, J.; Raghavachari, K.; Rendell, A.; Burant, J. C.; Iyengar, S. S.; Tomasi, J.; Cossi, M.; Rega, N.; Millam, N. J.; Klene, M.; Knox, J. E.; Cross, J. B.; Bakken, V.; Adamo, C.; Jaramillo, J.; Gomperts, R.; Stratmann, R. E.; Yazyev, O.; Austin, A. J.; Cammi, R.; Pomelli, C.; Ochterski, J. W.; Martin, R. L.; Morokuma, K.; Zakrzewski, V. G.; Voth, G. A.; Salvador, P.; Dannenberg, J. J.; Dapprich, S.; Daniels, A. D.; Farkas, Ö.; Ortiz, J. V.; Cioslowski, J.; Fox, D. J. Gaussian 09, revision D.01; Gaussian, Inc.: Wallingford, CT, 2009.
- (36) Olowookere, F. V.; Al Alshaikh, A.; Bara, J. E.; Turner, C. H. Effects of chain length on the structure and dynamics of polyvinyl chloride during atomistic molecular dynamics simulations. *Mol. Simul.* **2023**, *49* (15), 1401–1412.

- (37) Martínez, L.; Andrade, R.; Birgin, E. G.; Martínez, J. M. PACKMOL: A package for building initial configurations for molecular dynamics simulations. *J. Comput. Chem.* **2009**, 30 (13), 2157–2164.
- (38) Wypych, G. 3 PVC Additives. In *PVC Formulary*, 3rd ed.; ChemTec Publishing: Toronto, Canada, 2020; pp 47–94.
- (39) Abraham, M. J.; Murtola, T.; Schulz, R.; Páll, S.; Smith, J. C.; Hess, B.; Lindahl, E. GROMACS: High performance molecular simulations through multi-level parallelism from laptops to supercomputers. *SoftwareX* **2015**, *1*, 19–25.
- (40) Humphrey, W.; Dalke, A.; Schulten, K. VMD: visual molecular dynamics. *J. Mol. Graphics* **1996**, *14* (1), 33–38.
- (41) Bussi, G.; Donadio, D.; Parrinello, M. Canonical sampling through velocity rescaling. *J. Chem. Phys.* **2007**, *126* (1), 014101.
- (42) Nosé, S.; Klein, M. Constant pressure molecular dynamics for molecular systems. *Mol. Phys.* **1983**, *50* (5), 1055–1076.
- (43) Darden, T.; York, D.; Pedersen, L. Particle mesh Ewald: An Nlog (N) method for Ewald sums in large systems. *J. Chem. Phys.* **1993**, 98 (12), 10089–10092.
- (44) Hess, B.; Bekker, H.; Berendsen, H. J.; Fraaije, J. G. LINCS: A linear constraint solver for molecular simulations. *J. Comput. Chem.* 1997, 18 (12), 1463–1472.
- (45) Tribello, G. A.; Bonomi, M.; Branduardi, D.; Camilloni, C.; Bussi, G. PLUMED 2: New feathers for an old bird. *Comput. Phys. Commun.* **2014**, *185* (2), 604–613.
- (46) Santos, M.; Tavares, F.; Biscaia, E., Jr Molecular thermodynamics of micellization: micelle size distributions and geometry transitions. *Braz. J. Chem. Eng.* **2016**, *33*, 515–523.
- (47) Flory, P. J. Thermodynamics of high polymer solutions. J. Chem. Phys. 1942, 10 (1), 51–61.
- (48) Becker, S.; Urbassek, H. M.; Horsch, M.; Hasse, H. Contact Angle of Sessile Drops in Lennard-Jones Systems. *Langmuir* **2014**, *30* (45), 13606–13614.
- (49) Murray, J. S.; Brinck, T.; Lane, P.; Paulsen, K.; Politzer, P. Statistically-based interaction indices derived from molecular surface electrostatic potentials: a general interaction properties function (GIPF). J. Mol. Struct.: THEOCHEM 1994, 307, 55–64.
- (50) Lu, T.; Chen, F. Multiwfn: A multifunctional wavefunction analyzer. J. Comput. Chem. 2012, 33 (5), 580-592.
- (51) Bader, R. F.; Carroll, M. T.; Cheeseman, J. R.; Chang, C. Properties of atoms in molecules: atomic volumes. *J. Am. Chem. Soc.* 1987, 109 (26), 7968–7979.
- (52) Barbosa, G. D.; Liu, X.; Bara, J. E.; Weinman, S. T.; Turner, C. H. High-salinity brine desalination with amine-based temperature swing solvent extraction: A molecular dynamics study. *J. Mol. Liq.* **2021**, 341, 117359.
- (53) Liu, X.; Turner, C. Electronic structure calculations of the fundamental interactions in solvent extraction desalination. *J. Mol. Liq.* **2022**, *364*, 119986.
- (54) Barbosa, G. D.; Dach, E.; Liu, X.; Yip, N. Y.; Turner, C. H. Computational and experimental study of different brines in temperature swing solvent extraction desalination with amine solvents. *Desalination* **2022**, 537, 115863.
- (55) Mohammadi, M.; Fazli, H.; Karevan, M.; Davoodi, J. The glass transition temperature of PMMA: A molecular dynamics study and comparison of various determination methods. *Eur. Polym. J.* **2017**, *91*, 121–133.
- (56) Lindström, A.; Hakkarainen, M. Environmentally friendly plasticizers for poly (vinyl chloride)—Improved mechanical properties and compatibility by using branched poly (butylene adipate) as a polymeric plasticizer. *J. Appl. Polym. Sci.* **2006**, *100* (3), 2180–2188.
- (57) Rohling, J.; Medina, A.; Pereira, J.; Rubira, A.; Bento, A.; Miranda, L.; Baesso, M. Thermal lens versus DSC measurements for glass transition analysis of polymer. *Analytical Sciences/Supplements* **2002**, *17*, s103–s105.
- (58) Ziska, J.; Barlow, J.; Paul, D. Miscibility in PVC-polyester blends. *Polymer* **1981**, 22 (7), 918–923.
- (59) Altenhofen da Silva, M.; Adeodato Vieira, M. G.; Gomes Macumoto, A. C.; Beppu, M. M. Polyvinylchloride (PVC) and natural

- rubber films plasticized with a natural polymeric plasticizer obtained through polyesterification of rice fatty acid. *Polym. Test.* **2011**, *30* (5), 478–484
- (60) Wang, Y.; Zhou, C.; Xiao, Y.; Zhou, S.; Wang, C.; Chen, X.; Hu, K.; Fu, X.; Lei, J. Preparation and evaluation of acetylated mixture of citrate ester plasticizers for poly (vinyl chloride). *Iran. Polym. J.* **2018**, 27, 423–432.
- (61) Henson, W. R.; Rorrer, N. A.; Meyers, A. W.; Hoyt, C. B.; Mayes, H. B.; Anderson, J. J.; Black, B. A.; Jayakody, L.; Katahira, R.; Michener, W. E.; VanderWall, T. A.; Salvachua, D.; Johnson, C. W.; Beckham, G. T. Bioconversion of wastewater-derived cresols to methyl muconic acids for use in performance-advantaged bioproducts. *Green Chem.* 2022, 24 (9), 3677–3688.
- (62) Gilbert, M. PVC/plasticizer compatibility. III: Dynamic mechanical and tensile. *Plast., Rubber Compos. Process. Appl.* **1991**, 15 (4), 207–212.
- (63) Erythropel, H. C.; Maric, M.; Cooper, D. G. Designing green plasticizers: influence of molecular geometry on biodegradation and plasticization properties. *Chemosphere* **2012**, *86* (8), 759–766.
- (64) Sinisi, A.; Degli Esposti, M.; Toselli, M.; Morselli, D.; Fabbri, P. Biobased Ketal-Diester Additives Derived from Levulinic Acid: Synthesis and Effect on the Thermal Stability and Thermo-Mechanical Properties of Poly (vinyl chloride). ACS Sustainable Chem. Eng. 2019, 7 (16), 13920–13931.
- (65) Beirnes, K. J.; Burns, C. M. Thermal analysis of the glass transition of plasticized poly (vinyl chloride). *J. Appl. Polym. Sci.* 1986, 31 (8), 2561–2567.
- (66) Yin, B.; Hakkarainen, M. Oligomeric isosorbide esters as alternative renewable resource plasticizers for PVC. *J. Appl. Polym. Sci.* **2011**, *119* (4), 2400–2407.
- (67) McGinty, K. M.; Brittain, W. J. Hydrophilic surface modification of poly(vinyl chloride) film and tubing using physisorbed free radical grafting technique. *Polymer* **2008**, *49* (20), 4350–4357.
- (68) Sato, T.; Tsujita, Y.; Takizawa, A.; Kinoshita, T. Miscibility and volume changes of mixing in the poly (vinyl chloride)/poly (methyl methacrylate) blend system. *Macromolecules* **1991**, 24 (1), 158–160.
- (69) Righetti, M. C.; Cardelli, C.; Scalari, M.; Tombari, E.; Conti, G. Thermodynamics of mixing of poly (vinyl chloride) and poly (ethylene-co-vinyl acetate). *Polymer* **2002**, *43* (18), 5035–5042.
- (70) Lee, S.; Goo Lee, J.; Lee, H.; Mumby, S. J. Molecular dynamics simulations of the enthalpy of mixing of poly (vinyl chloride) and aliphatic polyester blends. *Polymer* **1999**, *40* (18), 5137–5145.
- (71) Etxeberria, A.; Iriarte, M.; Iruin, J. Enthalpies of mixing in polymer blends of chlorinated polymers: application of a group contribution method. *Macromolecules* **1995**, 28 (2), 589–595.
- (72) Brown, H.; Musindi, G.; Stachurski, Z. Effect of plasticizer concentration and annealing on the structure of PVC. *Polymer* **1982**, 23 (10), 1508–1514.
- (73) Fekete, E.; Foldes, E.; Pukanszky, B. Effect of molecular interactions on the miscibility and structure of polymer blends. *Eur. Polym. J.* **2005**, *41* (4), 727–736.
- (74) Kendall, M. J.; Siviour, C. R. Rate dependence of poly (vinyl chloride), the effects of plasticizer and time-temperature superposition. *Proceedings of the Royal Society A: Mathematical, Physical and Engineering Sciences* **2014**, 470 (2167), 20140012.
- (75) Zhou, Y.; Milner, S. T. Average and local T g shifts of plasticized PVC from simulations. *Macromolecules* **2018**, *51* (10), 3865–3873.